Fibers and Polymers 2019, Vol.20, No.3, 490-500
DOI 10.1007/s12221-019-8939-3

ISSN 1229-9197 (print version)
ISSN 1875-0052 (electronic version)

Polyurethane/Gelatin Nanofiber Neural Guidance Conduit in Combination with Resveratrol and Schwann Cells for Sciatic Nerve Regeneration in the Rat Model

Majid Salehi[1,2]*, Arian Ehtrami[3], Farshid Bastami[4,5], Saeed Farzamfar[6], Sepanta Hosseinpour[4], Hamid Vahedi[7], Ahmad Vaez[6], Mostafa Rahvar[8], and Arash Goodarzi[6]

[1]*Department of Tissue Engineering, School of Medicine, Shahroud University of Medical Sciences, Shahroud 3614773955, Iran*
[2]*Tissue Engineering and Stem Cells Research Center, Shahroud University of Medical Sciences, Shahroud 3614773955, Iran*
[3]*Department of Mechanical and Aerospace Engineering, Science and Research Branch, Islamic Azad University, Tehran 1477893855, Iran*
[4]*Dental Research Center, Research Institute of Dental Science, School of Dentistry, Shahid Beheshti University of Medical Sciences, Tehran 1983963113, Iran*
[5]*Oral and Maxillofacial Surgery Department, School of Dentistry, Shahid Beheshti University of Medical Sciences, Tehran 1983963113, Iran*
[6]*Department of Tissue Engineering and Applied Cell Sciences, School of Advanced Technologies in Medicine, Tehran University of Medical Sciences, Tehran 1417755469, Iran*
[7]*Clinical Research Development Unit, Imam Hossein Hospital, Shahroud University of Medical Sciences, Shahroud 3614773955, Iran*
[8]*Department of Medical Nanotechnology, School of Advanced Technologies in Medicine, Tehran University of Medical Sciences, Tehran 1417755469, Iran*

(Received October 9, 2018; Revised December 16, 2018; Accepted December 20, 2018)

Abstract: Peripheral nerve injury is a serious challenge which influences 2.8 percent of trauma patients. Tissue engineering of peripheral nerves mainly focuses on axonal regeneration via various nerve guides. The aim of this study is to evaluate a novel polyurethane (PU)/gelatin nanofibers (GNFs) conduit's potential combination with resveratrol (RVT) for sciatic nerve regeneration in the rat. Platelet-rich plasma (PRP) was used as a carrier for RVT. Different tests like contact angle, tensile strength etc. was used to evaluate properties of PU/GNFs conduits. In addition, the electron microscopy, MTT assay, and DAPI staining revealed its compatibility with Schwann cells. 24 male Wistar rats were allocated into four groups (n=6) (1) PU/GNF/PRP/Schwann cell, 2) PU/GNF/Schwann cell/PRP/RVT, 3) Positive control, and 4) Negative control in order to assess sciatic functional index (SFI), hot plate latency, electromyographical (EMG), the percentage of wet weight-loss of gastrocnemius muscle and histopathological studies using hematoxylin-eosin staining. The results represented sciatic functional index (SFI), hot plate latency, electromyographical improved significantly in group 1 and 2 compared to the negative control group. Histopathological findings showed remarkable improvements in myelin sheath regeneration and fibers condition in group 1 and 2 compared to the negative control group. Group 2 showed more resemblance to the normal sciatic nerve, with well-arranged fibers and an intact myelin sheath. This study successfully applied PU/GNFs/PRP/RVT conduits as a potential biocompatible nerve guide with proper mechanical properties, biocompatibility, and biodegradability that enhanced injured sciatic nerve's recovery rate.

Keywords: Polyurethane, Gelatin nanofibers, Resveratrol, Neural guidance conduit, Schwann cells

Introduction

Peripheral nerve injury is a serious challenge which influences 2.8 percent of trauma patients [1] and approximately more than 660000 new cases of peripheral nerve injuries occur in the United States and Europe annually [2]. Despite the healing potential in peripheral nerves, functional recovery may not be satisfactory. Application of autologous nerve graft is the gold standard treatment modality for bridging nerve gap [3]. However, this approach has some shortcomings which include the shortage of available graft tissue, morbidity of the donor site, and inappropriate size and structure [2,4]. Therefore, finding alternative solutions is highly demanded. Tissue engineering of peripheral nerves mainly focuses on axonal regeneration via various nerve guides [5-8]. Researchers introduced artificial neural guidance conduits (NGCs) as a substitute for their ease of mass production [9]. Despite of their useful properties, current designs are not as efficacious as autografts and are limited because of a narrow range of options [10]. Thus, improving NGCs that can match the effectiveness of an autologous nerve graft would be useful in the field of peripheral nerve surgery.

Fabrication of a nerve guide requires a proper biocompatible and biodegradable material. There are a considerable number of natural and synthetic materials such as hyaluronic acid [11], fibrin [12,13], collagen [14], gelatin [15], polyurethane (PU) [16], poly(lactide-ε-caprolactone) [17], poly(glycolic acid) [18,19], poly(DL-lactic-co-glycolic acid) [20], and poly(L-lactic acid) [21], that individually represent

*Corresponding author: salehi.m@shmu.ac.ir

various advantages. For instance, natural biomaterials indicated appropriate biocompatibility and biologic function and synthetic biomaterials represented proper mechanical strength, controllable porosity and degradation rate [22]. However, natural biomaterials showed insufficient mechanical strength and too fast biodegradation rate, and synthetic biomaterials demonstrate lower biocompatibility, high hydrophobicity, and inflammatory reactions [22]. Nowadays, nanofibers have attracted attention because these nanostructures are highly similar to the structural hierarchy of the extracellular matrix [23]. Polyurethanes are synthetic polymers which are widely used in a variety of applications due to their extensive structural/property diversity like good biocompatibility, appropriated mechanical properties, elasticity and flexibility and high elongation [24]. Synthetic polymers have poor cell affinity because of their low hydrophilicity and lack of surface cell-recognition sites. To improve the cell-synthetic polymer interactions, the hydrophilic property and incorporation of cell-recognition sites such as RGD (Arg-Gly-Asp) and extracellular matrix (ECM) bioactive proteins have been used [25]. Gelatin is a natural polymer which is derived from collagen and has an almost same composition as collagen [26]. The use of gelatin as a conduit material decline the concerns of immunogenicity and pathogen transmission associated with collagen [27,28]. One of the potential strategies for adding gelatin into NGCs is to incorporate it in the form of nanofibrils into NGCs. This small dimension of fibrils can physically mimic the structural properties of native ECM [29].

Structures of NGCs can be designed to meet different kinds of requirements such as porous and fibrillated structures with good permeability and degradability, along with suitable mechanical properties to resist collapse when they are used in vivo [22]. Electrospinning and thermally induced phase separation (TIPS) are widely used to produce such structures [9,30]. Electrospinning is a process that can produce nanofibrillated structures that mimic the ECM [31], on the other hand, the TIPS can fabricate porous structures with high permeability to nutrients [32].

These days, enrichment of NGCs' structures with factors that can improve the outgrowth of axons has been used as a strategy to enhance the peripheral nerve repair [33]. Resveratrol (RVT) is a natural polyphenolic antioxidant which has been suggested as a neuroprotective agent [34-36]. Wang *et al.* reported its beneficial impact on insulin-like growth factor-1 signaling (IGF-1) in the animal model [37]. In addition, Bagriyanik *et al.* in 2014 showed RVT's therapeutic effect on sciatic nerve-injured rats [38]. They reported an increased level of IGF-1 expression when RVT applied. However, the exact molecular mechanism of RVT in nerve regeneration is still unclear. Another agent that has positive effects on neural repair is platelet-rich plasma (PRP) [39]. The improving effect of PRP is based on the premise that a large number of platelets in the PRP release a high amount of growth factors that help the healing process. These growth factors action locally to attract undifferentiated cells to the site of injury, start mitosis in these cells, and induce angiogenesis [40]. Another strategy which is used to enhance the peripheral nerve repair is cell therapy that shows a powerful approach to repair the neural damages [41]. Schwann cells (SCs) preserve and myelinate nerve fibers of the peripheral nerve system. SCs produce specific extracellular matrix proteins and release neurotrophic factors for nerve regeneration [42]. It has been shown that the Schwann cells are important for nerve regeneration following nerve injury. They have an essential role in the axonal regeneration that stimulate proliferation and activation of Schwann cells in the injured nerve fibers and synthesis of S-100 protein [43].

In the present study, an NGC was fabricated from polyurethane and gelatin nanofibrils via the combination of electrospinning and TIPS techniques for transplantation of SCs. During the implantation, NGCs were seeded with SCs and filled with PRP gel containing RVT. This conduit had a structural guidance for axonal regeneration, as well as a carrier for therapeutic agents and SC transplantation. It was used in a rat sciatic nerve defect, which simulates the clinical long-gap peripheral nerve injury, to evaluate its ability to support the neural repair in clinical settings.

Experimental

Chemicals

The materials and solvents were purchased from Sigma-Aldrich (St. Louis, USA) and Merck (Darmstadt, Germany) respectively unless otherwise noted.

Preparation of Conduits

Gelatin Nanofibers (GNF) Preparation via Electrospinning

Gelatin solution (bovine skin type B) (Sigma Co., St. Louis, USA) with a concentration of 40 % (w/v) were processed by mixing aqueous acetic acid and water with the ratio (75/25, % v/v) as solvent at room temperature. Electrospinning was performed by applying a positive high voltage of 20 kV to the metal needle of a 10 m*l* syringe with 18-gauge metal needle, and a counter electrode at about 15 cm apart from the capillary tip. Then, the loaded syringe placed into a feeding pump (SP1000, Fanavaran Nano-Meghyas, Iran) with 0.5 m*l*/h feeding rate. The extruded solution was collected on an aluminium-foil at room temperature. Drum's turning rate was 450-500 rpm. The acquired nanofibers transferred to a liquid nitrogen tank and preserved for 24 hours. The fibers were crushed and kept at 4 ºC immediately after removing from the tank. At the end, the crushed gelatin nanofibers cross-linked by the vapour of glutaraldehyde 15 % for 24 hours and then rinsed with distilled water.

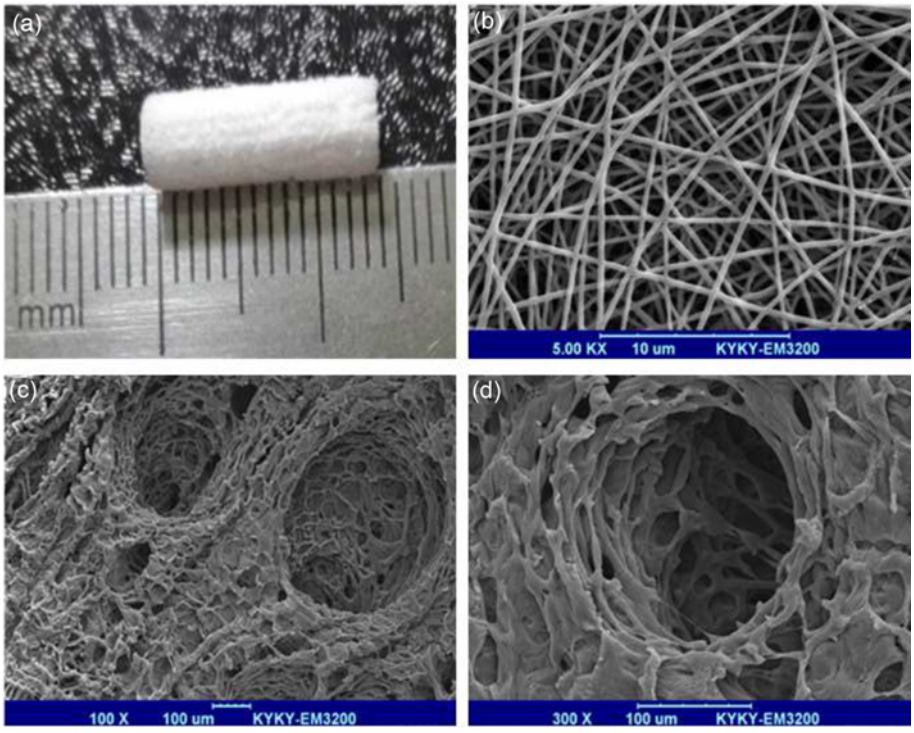

Figure 1. (a) Fabricated polyurethane/gelatin nanofibers conduit, (b) scanning electron microscope (SEM) image of gelatin nanofibers prepared by electrospinning, and (c, d) SEM image of polyurethane/gelatin nanofibers conduit.

Conduits Fabrication by Thermally Induced Phase Separation Method

Gelatin nanofibers (GNFs) were synthesized with gelatin solution (bovine skin type B) (Sigma Co., St. Louis, USA) with the concentration of 40 % (w/v). The acquired gelatin nanofibers were transferred to a liquid nitrogen tank and preserved for 24 hours. The fibers were crushed and kept at 4 ^{o}C immediately after removing from the tank. The polymer solution was prepared by mixing polyurethane (PU) with a total concentration of 6 % (w/v) in 1,4-Dioxane for 24 hours. The prepared GNFs were dispersed in PU solution at the weight ratio of 80:20 (PU: GNF). In order, to initiate phase separation, the solutions quenched from 24 ^{o}C to -80 ^{o}C on account of the solvent freezing point (~12 ^{o}C) and maintained for about three hours. Then, specimens were freeze-dried instantly by a freeze dryer at -70 ^{o}C (121550PMMA, Christ, Spain) for 48 hours [44]. Finally, customized conduits with 14 mm length, 3 mm outer diameter and 1 mm inner diameter were fabricated using a water jet machine (Figure 1(a)).

Scaffold Characterization

Scanning Electron Microscopy

A scanning electron microscope (SEM) (DSM 960A, Zeiss, Germany) was utilized to determine the morphology of fabricated scaffolds. All samples were perceived under SEM at 26 kV and were coated with gold for 180 seconds using a sputter coater (SCD 004, Balzers, Germany).

Porosity Assessment

To determine the porosity of the conduits, liquid displacement and equation (1) were used [45];

$$\text{Porosity (\%)} = \frac{V_1 - V_3}{V_2 - V_3} \quad (1)$$

V_1 indicates the volume of ethanol (96 %) prior to conduits immersion, V_2 is the volume after immersing the scaffold, and V_3 stands for the volume of the ethanol after the conduits removal (after 10 min).

Contact Angle Measurement

In order to determine the hydrophilicity of the scaffold, static contact angle assessed using a static contact angle measuring device (KRUSS, Hamburg, Germany) [46].

Weight Loss Measurement

To determine in vitro degradation rate, the specimens were cut and immersed in 10 m*l* of phosphate buffered saline (PBS) at 37 ^{o}C in a water bath for 30 and 60 days. After each incubation period, conduits were taken out and weighed after drying in vacuum for 2 days. This remaining weight was measured as the percent of the original dry scaffold weight found at each time point (n=3). The percentage of weight loss was calculated by the following equation [47]:

$$\text{Weight loss (\%)} = \frac{W_0 - W_1}{W_0} \times 100 \quad (2)$$

W_0: The initial weight of samples and W_1: The dry weight

after removing from the media.

Mechanical Properties

Tensile strength and Young's modulus was measured on dry rectangular specimens (80×10 mm) by an Instron 5566 universal testing machine (Instron, MA) (strain rate=10 mm/min). All tests performed three times.

Schwann Cell Isolation and Culture

Primary Schwann cells (SCs) of 8-10 day old postnatal Wistar rat was isolated from sciatic nerves (School of Medicine of Shahroud University of Medical Sciences, Shahroud, Iran) using modified Brockes method [48,49]. The harvested cells were cultured in Dulbecco's modified Eagle's medium: nutrient mixture F-12 (DMEM/F12; Gibco, Grand Island, USA), 100 unit/m*l* of penicillin, 100 μg/m*l* of streptomycin, and supplemented with 10 % (v/v) fetal bovine serum (FBS; Gibco, Grand Island, USA) in a humidified incubator at 37 °C with 5 % CO_2. The culture medium repeatedly replaced every 48 hours. Prior to cell seeding, the conduits in a 96-well plate were sterilized by ultraviolet light irradiation for 60 min and then seeded with 1×10^4 third passage cells.

Cell-scaffold Interaction Studies

To assess the morphology of SCs on the conduit material, SCs were seeded onto the conduits at the density of 1×10^4 cells per sample and cultured for 24 h. After this incubation period, the cells on the scaffolds were fixed by 2 % Paraformaldehyde and 2.5 % Glutaraldehyde for 60 minutes at 4 °C. For dehydration, the specimen wash twice in PBS to remove fixative from the sample and then dehydration was performed in a series of increasing concentrations of ethanol in distilled water 30 %, 50 %, 70 %, 95 %, and 100 % for 10 min per each concentration. The samples were dried in air for 24 h. Finally, conduits were sputter-coated with gold and observed under SEM (DSM 960A, Zeiss, Germany).

The proliferation of SCs on the matrices was assessed by MTT assay (Sigma, St. Louis, Missouri, United States). After 48 and 72 h, added 50 μ*l* of serum-free media and 50 μ*l* of MTT solution (5 mg/m*l*) into each well containing cell-scaffold constructs and incubated for 4 h at 37 °C. After this incubation period, the supernatant was discarded and 100 μ*l* dimethyl sulfoxide (DMSO) (Roche, Basel, Switzerland) was added to each well to dissolve any formed formazan crystals. The absorbance values were read at 570 nm using a microplate reader (Stat fax-2100, Awareness Technology Inc., Palm City, FL, USA) [50].

DAPI (4',6-diamidino-2-phenylindole dihydrochloride) (DAPI, Sigma Aldrich, USA) staining was used to visualize SCs attached to the scaffold after 48 hours of cell seeding. To illustrate, after fixing the cells seeded on the scaffolds (60 μ*l*/well of 4 % Paraformaldehyde for 8 minutes), 0.1 % Triton-X-100 was poured on the scaffold to increase the dye penetration. DAPI solution (concentration 1:1000) was added to the scaffolds and kept for 5 min at room temperature. Unbonded DAPI was removed by washing it thrice with PBS [47]. To keep the cells hydrated while imaging added 50 μ*l*/well of 1x PBS.

In vivo Investigation

Animal

All the procedures in these experiments were approved by the ethical committee of Shahroud University of medical sciences, Shahroud, Iran (ethical code: IR.SHMU.REC. 1397.098). 24 males adult Wistar rats weighing 200±250 grams were used to evaluate nerve regeneration. The animals were allocated into 4 groups (6 rats per group): 1) PU/GNF/Platelet-rich plasma (PRP)/Schwann cell group, 2) PU/GNF/Schwann cell/PRP/Resveratrol group, 3) Negative control (with nerve injury but without surgical interventions), 4) Positive control (rats without sciatic nerve injury). Prior to cell seeding in the PU/GNF/Platelet-rich plasma (PRP)/Schwann cell and PU/GNF/Schwann cell/PRP/Resveratrol groups, the conduits in a 24-well plate were sterilized by ultraviolet light irradiation for 60 min and then seeded with 1×10^4 third passage cells.

PRP Preparation

Kajikawa *et al.*'s [51] technique of harvesting PRP was used in the current study. Briefly, whole body blood of three donor rats was obtained via decapitation after scarification humanly. A mean of 7-8 m*l* blood sample was retrieved per rat and mixed with1 m*l* sodium citrate (3.8 % w/v) (Sigma, St Louis, Missouri) as an anticoagulant. After centrifugation at 1500 rpm for 10 minutes, the platelet-rich part was isolated the layer containing red blood cells. This platelet-rich sample was centrifuged at 3000 rpm for 10 minutes to form a pellet. The pellets were re-suspended and kept for further use. To activate the PRP 20 μ*l* of PRP was mixed with 3.33 μ*l* 300 IU thrombin (Sigma) and 3.33 μ*l* 10 % $CaCl_2$ (Sigma). In the group containing resveratrol, the PRP/resveratrol gel was prepared by blending 100 mg of resveratrol with 100 μ*l* of PRP and then 150 μ*l* of the PRP/Resveratrol gel was injected into the cell-seeded polyurethane/gelatin nanofibers conduits by needle 18 gauge before the distal nerve ending was sutured to the other end of the conduit.

Surgical Procedure

Animals were deeply anesthetized by intraperitoneal injection of Ketamine 60 mg/Xylazine 6 mg (kg body weight). The operation was conducted on the animals' left legs, under aseptic condition. Rat's skin was shaved and their sciatic nerve was exposed and a 10 mm nerve piece was removed with a micro scissor. The proximal and distal nerve stumps were sutured into the wall of the conduits with resorbable suture (Vicryl 6.0; Ethicon GmbH & Co. KG, Norderstedt, Germany) leaving a 10 mm gap between the two stumps.

Evaluation of Sciatic Function Index (SFI)

To quantification of the deficit in the descending fine motor, rats' footprints were obtained after 4 and 8 weeks post-surgery according to Dijkstra *et al.* [52] through the use

of millimeter paper strips that were engaged in a gait track built. After five minutes of primary gait training, the rats' paws were dyed by Nanjing ink and their footprints were registered for the SFI record. The two paws of animals were given two different colours, i.e. red and blue. Walking into an acrylic alley with specific size, the rats would step on the paper used to cover the alley's floor. Length calculation was conducted on various lines which encompass the distance from the heel to the top of the third toe [53], the line between the tips of the thumb and the little toe (TS), and the distance between the tips of the second and fourth toes (IT). Each was assessed on the right and left foot of animals' hind limbs during straight walking. Then, these measurements were introduced into a mathematical equation where the results showed the amount of the deficit in the harmed side (O= operated paw), compared to the normal side (N=normal paw). The normal function or the absence of injury was represented by an index of 0 while -100 revealed the through loss of function and complete nerve injury.

The SFI was calculated according to the equation:

$$SFI = -38.3\,[(OPL-NPL)/NPL] + 109.5\,[(OTS-NTS)/NTS] + 13.3\,[(OIT-NIT)/NIT] - 8.8.$$

Electrophysiological Assessment

Two months after surgery, electromyographical recordings were performed in all groups to measure the recovery of the motor system. The compound muscle action potential (CMAP) [54] of the gastrocnemius muscle were analyzed in this test by an electromyographic recorder (Negarandishegan, Tehran, Iran). The sciatic nerve just before the proximal part of the cut was triggered by an electric monophasic stimulus. To diminish any possible interference, a ground electrode was placed inside the muscle near the nerve. Cap electrodes situated on the gastrocnemius muscle to record the gastrocnemius response. A 2 cm distance between the site of stimulation and the muscle was kept constantly in all experiments.

Hot Plate Latency Test

The rats were evaluated for hot plate latency (HPL) by placing rats on a hot plate (56 ^{o}C) and recording the time until they jumped or licked their paws after 8 weeks. After their response, the rats were eliminated from the plate and the cut off time for their reaction was arranged at 12 seconds.

Gastrocnemius Muscle Mass

At the end of 8 weeks' post-surgery, animal models were euthanized and posterior gastrocnemius muscles on the operated and non-operated limbs were obtained and instantly weighed.

Histological Evaluation

The harvested tissues (sciatic nerve and gastrocnemius muscle) have fixed in the 10 % neutral buffered formalin (PH.7.26) for 48 h, and then the fixed harvested samples processed and embedded in paraffin. The 5 μm thick sections were prepared and stained with hematoxylin and eosin (H&E). Finally, the histological evaluation was done by the independent pathologist, using light microscopy (Olympus BX51; Olympus, Tokyo, Japan). For the nerve specimens, transverse sections were obtained from cutting area. The prepared slides were stained with hematoxylin and eosin (H&E). Finally, the histological slides were evaluated by the independent reviewer, using light microscopy (Olympus BX51; Olympus, Tokyo, Japan). The histo-morphometric analysis was also performed by measuring the cross-section areas of the muscle fibers.

Statistical Analysis

In this study, all the experiments were accomplished in triplicate and all data were analyzed by SPSS version 20.0.1 (IBM Corp., Armonk, NY, USA). Findings were compared between groups singly with analysis of variance ANOVA. For all comparisons, the degree of importance was $p \leq 0.05$ and Tukey's test was used as the post hoc.

Results and Discussion

Scaffold Characterization

Morphological Studies

The SEM image of the GNFs (Figure 1(b)) illustrated that the fibers had a uniform structure with smooth morphology and they were randomly distributed. The fibers' diameters and distributions were measured using ImageJ (National Institutes of Health, Bethesda, USA) using random assessing of 20 fibers per image, and they had the mean diameter of 328.00±61.29 nm. Figure 1(c) and 1(d) demonstrate the porous structure of the PU/GNFs conduit. The PU/GNFs conduits showed a porosity of 87.1 %±1.89 in comparison to a porosity of 89.11 %±2.03 for polyurethane conduits. Our findings showed that incorporation of GNFs into PU did not significantly affect the mean porosity percentage of the conduit.

Contact Angels' Results

The contact angle of PU/GNFs conduits was 78.3±2.52 degrees and its amount in polyurethane group was 103±2.35 degrees. GNFs incorporation significantly decreased the mean value of the contact angle ($p<0.001$).

Weight Loss Measurements

Table 1 summarizes the percentage of weight losses for both groups in various media. Incorporation of GNFs significantly enhanced the degradation of PU/GNFs conduit which was evidenced by its weight-loss values after 30 and 60 days. The differences between groups under experimental conditions were statistically significant ($p<0.05$) except the comparisons between PU/GNFs and polyurethane groups in 90 % DMEM/10 % FBS ($p>0.05$).

Mechanical Properties Results

Due to the fact that tensile properties have a direct impact on stability of NGCs, the enhanced tensile strength ameliorate the suturing process during the grafting surgery [55]. The tensile strength of PU/GNFs group was 5.4±0.98

Table 1. Weight loss of polyurethane/gelatine nanofibers and polyurethane groups in various media after 30 and 60 days

Sample	Medium	30 days (%)±standard deviation	60 days (%)±standard deviation
Polyurethane	90 % DMEM/10 % FBS	15.3±4.51	23.8±3.24
	DMEM	3.6±1.44	3.7±0.32
	DW	0.6±0.15	2.2±0.15
Polyurethane/gelatin nanofibers	90 % DMEM/10 % FBS	23.4±2.99	31.6±3.77
	DMEM	14.9±2.80	21.8±1.55
	DW	7.4±1.02	13.8±1.30

*Abbreviations: Dulbecco's modified Eagle's medium: DMEM; distilled water: DW; fetal bovine serum: FBS.

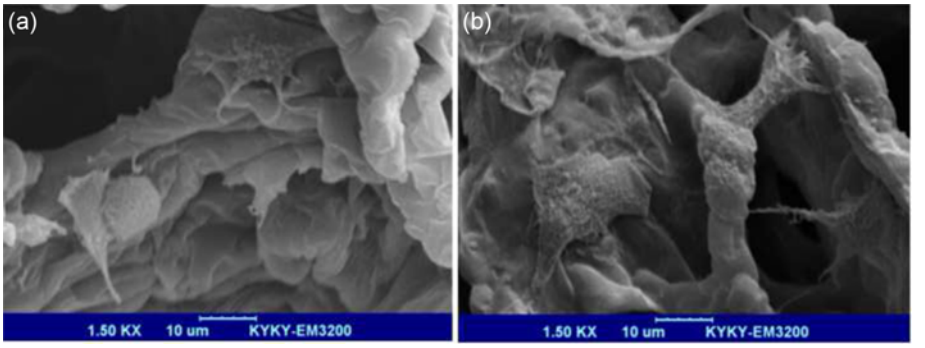

Figure 2. SEM images of SCs seeded on (a) PU group (b) PU/GNFs group.

MPa and tensile strength of PU group was 6.8±1.13 MPa (p=0.18). In addition, PU/GNFs group indicated lesser Young's modulus (3.1±0.65 GPa) compared to polyurethane group (3.54±1.03 GPa) with no statistically significant difference (p<0.56). Analysis of mechanical properties revealed that the GNFs incorporation decreased the ultimate tensile strength and the Young's Modulus of PU conduit results; however, these results were not statistically significant.

Cell-Scaffold Interactions

SEM images of SCs seeded on scaffolds revealed that the cells had an almost spherical morphology with poor spreading in PU group (Figure 2(a)). Although cell attachment can be seen in this group, because of PU's hydrophobicity, the attachment was not well developed. GNFs incorporation showed improved cell adhesion and spreading compared to PU conduit (Figure 2(b)). This may be due to the cell attachment sites present in gelatin which can improve the cell-conduits interactions.

Schwann Cells Viability

The scaffolds containing RSV had more cell viability (Figure 3). Incorporation of PRP and RSV with PU/GNFs conduit not only had no toxic effects on SCs but also this addition significantly promoted their expansion as confirmed by increasing their MTT absorbance values after 48 and 72 h compared to PU and control groups (p<0.05) (Figure 3).

DAPI Staining Results

Forty-eight hours after seeding of SCs on the conduits, a relatively higher number of visible SCs were present in PU/GNF/PRP/RSV (Figure 4(c)) in comparison with PU (Figure 4(a)) and PU/GNF/PRP (Figure 4(b)). These findings were in accordance with MTT and SEM observations. As can be seen in Figure 4, PU/GNF/PRP/RSV group provided a better surface for cell attachment than the other groups.

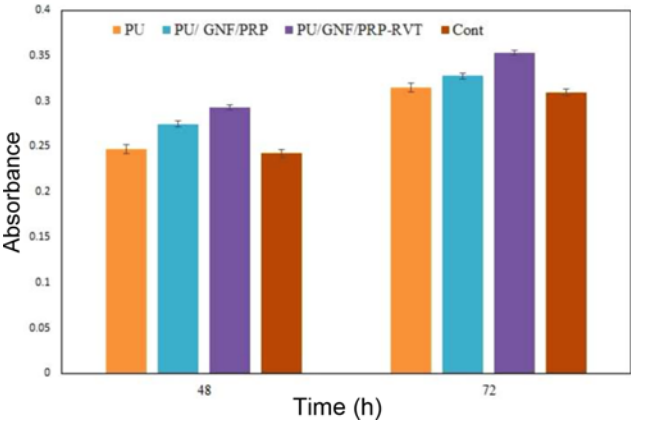

Figure 3. Evaluation of proliferation of Schwann cells in four different groups (polyurethane (PU)/gelatin nanofibers (GTNF)/ platelet rich plasma (PRP), PU/GTNF/PRP/Resveratrol, PU, and Control) by MTT assay after 48 and 72 hours.

In vivo Findings

Sciatic Function Index (SFI)

SFI values in experimental and control groups at two-time points are shown in Figure 5. In each time interval, the SFI values had the same trend and positive control>PU/GNFs/

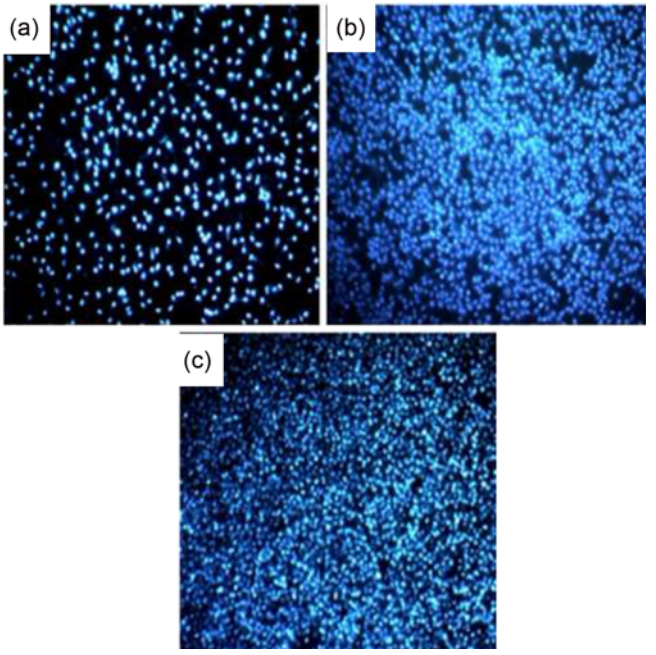

Figure 4. Representative images of DAPI staining of Schwann cells (a) PU, (b) PU/GNF/PRP, and (c) PU/GNF/PRP/Resveratrol.

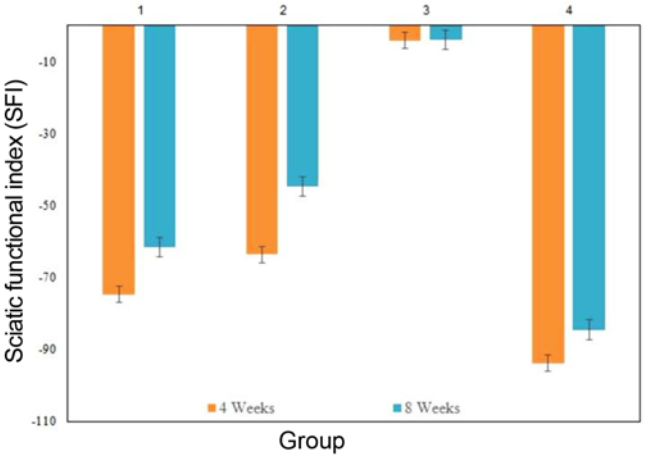

Figure 5. The sciatic function index (SFI) of groups after 4 and 8 weeks. Groups: 1) PU/GTNF/PRP/Schwann cell, 2) PU/GTNF/PRP/Schwann cell/Resveratrol, 3) positive control, and 4) negative control.

PRP/RSV/SCs>PU/GNFs/PRP/SCs>negative control. Group PU/GNF/PRP/Schwann cell and PU/GNF/PRP/Schwann cell//Resveratrol showed no significant differences at 4 weeks (-74.7±2.40 vs. -63.3±3.15) and 8 weeks (-61.5±3.5 vs. -41.4±1.49) ($p>0.05$).

Electrophysiological Assessment

In Figure 6 are the wave patterns of electrophysiological recordings of gastrocnemius muscle evoked potentials of implanted (Figure 6(a) and 6(b)) and controls (Figure 6(c) and 6(d)) two months after surgery. The mean peak

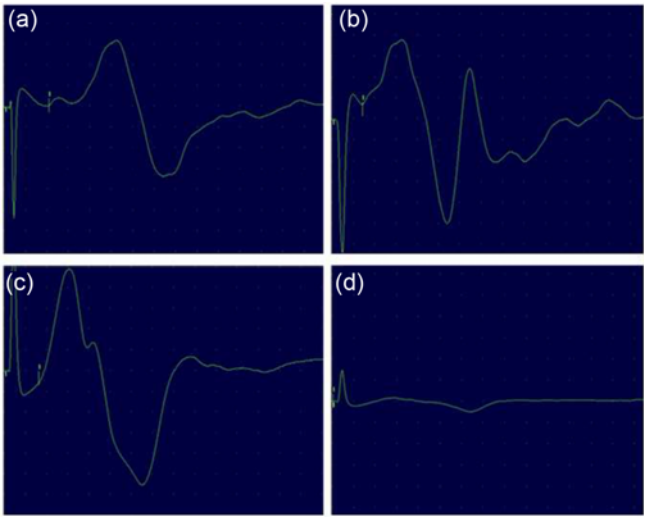

Figure 6. Electrophysiological recordings of gastrocnemius muscle evoked potentials from the implanted (a) PU/GTNF/PRP/Schwann cell, (b) PU/GTNF/PRP/Schwann cell/Resveratrol, (c) positive control, and (d) negative control two months after implantation.

amplitude in PU/GNF/Schwann cell/PRP (Figure 6(a)) and PU/GNF/Schwann cell/PRP/Resveratrol (Figure 6(b)) were 13.38±0.89 and 17.27±2.40, respectively. For the positive (Figure 6(c)) and negative controls (Figure 6(d)), the mean peak amplitude was 31.60±1.56 and 0.57±0.02 respectively. There was a statistically significant difference between Figure 6(a) and Figure 6(b) ($p<0.05$) and between experimental groups and the negative control group ($p<0.05$). Statistically, no significant difference was observed between experimental groups and the positive control group ($p<0.05$).

Hot Plate Latency Test

In order to assess the nociceptive function of nerves, HPL test was performed. The nociceptive function was significantly influenced by the sciatic nerve injury since the rats in the negative control group did not withdraw their paws from the hot plate within 12 seconds. Rats in group PU/GNF/Schwann cell/PRP/Resveratrol had the smallest HPL time (6-8 s) among experimental groups. In the hot plate latency time, all differences among the groups were statistically significant ($p<0.05$) (Table 2).

Table 2. Hot-plate latency time in study groups

Group	Latency time (seconds)
Polyurethane (PU)/gelatin nanofibers (GTNF)/ platelet rich plasma (PRP)/Schwann cell	9.5 (9-10)
PU/GTNF/Schwann cell/PRP/Resveratrol	7 (6-8)
Positive control	3.5 (3-4)
Negative control	12 (12-12)

*Data is represented as median (Min-Max).

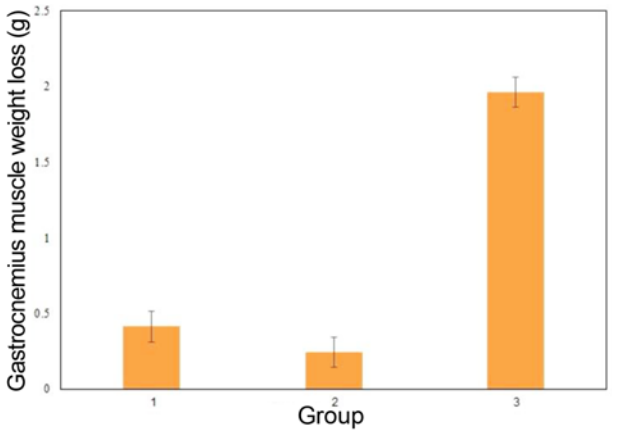

Figure 7. Histogram comparing the gastrocnemius muscle wet weight (g) between operated side (left) and normal side (right) in all groups 8 weeks post-surgery. Groups: 1) PU/GTNF/PRP/Schwann cell, 2) PU/GTNF/Schwann cell/PRP/Resveratrol, and 3) negative control.

Gastrocnemius Muscle Wet Weight-loss

Gastrocnemius muscle wet weight-loss has been reported as a consequence of denervation that indirectly reflects the motor neuron defect [56]. This is a reversible process and muscle atrophy can be stopped if the muscle is re-innervated [57]. The percentage of the wet weight loss of the gastrocnemius muscle indirectly indicates the extent of muscle re-innervation. The mean of gastrocnemius muscle weight was measured (Figure 7). There was a statistically significant difference in muscle weights between operated sides of all groups and negative group ($p<0.05$). There was no statistically significant difference between PU/GNF/Schwann cell/PRP/Resveratrol and PU/GNF/Schwann cell/PRP groups ($p>0.05$).

Histological Findings

Histological Changes in Injured Sciatic Nerve

The histopathological evaluation of group 1 (PU/GNF/Schwann cell/PRP) showed myelin vacuolation and mild edema around neuronal fibers. Histological assessment of group 2 (PU/GNF/Schwann cell/PRP/Resveratrol) revealed remarkable improvements in myelin sheath regeneration and fibers condition. The signs of nerve injury were diminished and only mild vacuolation was evident in this group. Among these two treatments, the micrographs of group 2 improved all the histological changes following the damage and showed more resemblance to the normal sciatic nerve, with well-arranged fibers and intact myelin sheath. Histopathological evaluation of the positive control group showed well-arranged myelinated fibers without any sign of nerve damage. In the nerve injury model (negative control) group, the fibers' arrangement was disturbed and they had swollen or missing axons with various degrees of edema and vacuolation. Severe histopathological damages including a breakdown of the myelin sheath, degenerated nerve fibers, perineural fibrosis, axonopathy and notable edema of the nerve fibers were observed in this group (Figure 8).

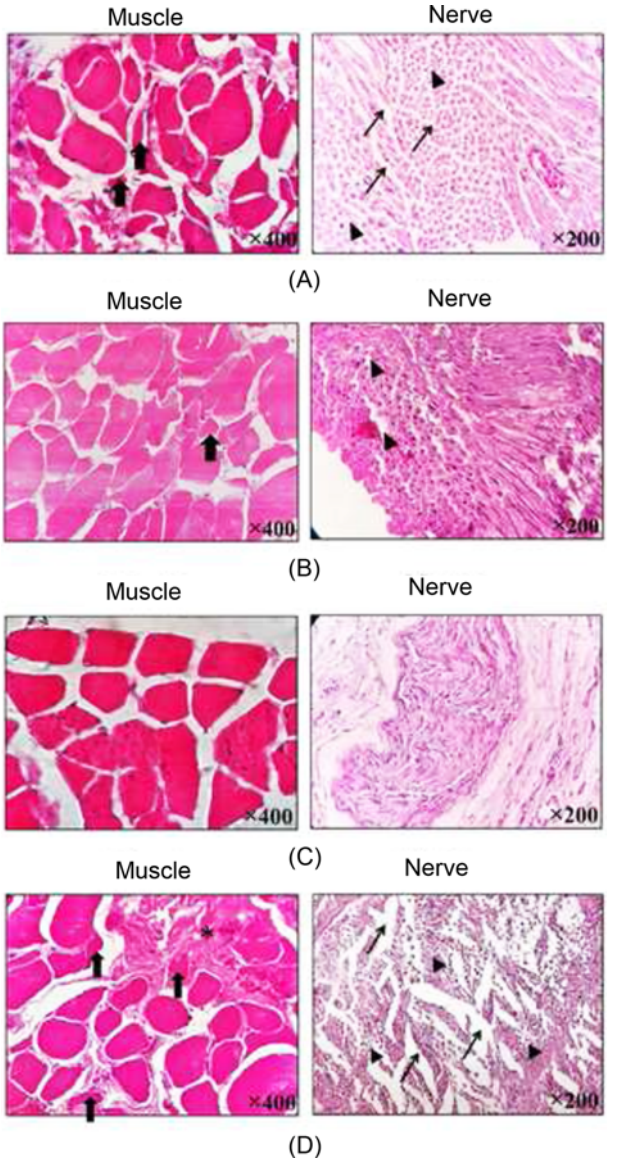

Figure 8. Histopathological images of the sciatic nerve and gastrocnemius muscle (×400) cross-sections stained by hematoxylin-eosin (H&E) at the end of 8th week post-surgery; (A) PU/GTNF/PRP/Schwann cell, (B) PU/GTNF/Schwann cell/PRP/resveratrol, (C) positive control, and (D) negative control. Arrowheads: focal epineurium loss, asterisks: collagen hyperplasia, narrow arrows: vacuolation, thickened arrows: atrophied muscle fiber.

Histopathological Changes of Gastrocnemius Muscle Post-sciatic Nerve Injury

Cross-sectional areas of muscle were 2682±174 mm^2 in positive control group, 793±42 mm^2 in negative control group, 1951±106 mm^2 in group 1 (PU/GNF/Schwann cell/

PRP), and 2216±149 mm^2 in group 2 (PU/GNF/Schwann cell/PRP/Resveratrol). In group 1, some of the muscular cells were atrophied and fibrosis was seen between the muscular fibers. However, the muscular damaged was significantly reduced in comparison to the negative control. The muscular cells of group 2 (PU/GNF/Schwann cell/PRP/Resveratrol) restored normal condition; however, atrophy was still present in some myocytes. In overall, the muscle fibers in group 2 were more similar to the normal group than others (Figure 8). The cross-sectional area of the muscle bundles was evaluated by image processing software (image pro-plus software, version 6, Cybernetic, USA) and reported for each group. The cross-sectional area was the greatest in the positive control group. In addition, this area was greater in group 2 than 1 and negative control groups. The histopathological evaluation of positive control group, muscle fibers revealed an intact gastrocnemius muscle which presented by plump and red in color muscle fibers. On the other hand, the evaluation of gastrocnemius in the negative control group showed atrophied, broken and wiggly muscle fibers. In addition, the myocytes striation was disappeared and hyalinization of the muscle fibers was evident. The proliferation of collagen fibers (fibrosis) is considerably increased between muscle bundles and the organization of gastrocnemius muscle was completely distorted.

An ideal nerve guide should possess many requirements. The microstructure is one of the most imperative characteristics of a scaffold which secures Schwan cells and axons to receive nutrients and essential bioactive molecules. Hydrophilicity of a scaffold by altering the amount of water absorption and permeability plays a pivotal role especially for *in vivo* application. Hydrophilicity need to be adjusted precisely due to at both low and high ranges can be destructive and may result in less cell attachment, excessive swelling, and poor mechanical strength. Cui *et al.* indicated that incorporation of 1-2 % collagen into pure PU enhanced its water absorbability with acceptable compressive strength [22]. In this study, we decreased the amount of contact angle (78.3±2.52 ^{o}) by adding gelatin nanofibers to polyurethane for ameliorating the hydrophilicity of the conduit. Gelatin has a high water solubility that renders appropriate processing in water solutions; however, it provides poor mechanical properties [58,59]. Therefore, crosslinking this material with other proper agents can potentially make a proper structure for nerve regeneration. In this study like our previous research [60], adding gelatin nanofibers (weight ratio of 80 PU:20 GNFs) not only improved hydrophilicity but also altered tensile strength and Young's modulus with no significant difference compared to pure PU. Farzamfar *et al*. [25] also showed the most favorable ratio of electrospun poly(caprolactone) (PCL)/gelatin that represented the most balanced characteristics was 80:20.

Schwann cells are prerequisite for regeneration and repair of peripheral nerves. Currently, these cells have been implanted separately or in conjunction with biomaterials as nerve guide conduits [61]. In fact, inducing and stimulating Schwann cells can improve nerve regeneration especially in peripheral nerves injuries [62]. In the current study, we applied PRP as a carrier for RVT. PRP is a natural source of a plethora of growth factors which have been successfully applied for intensifying nerve regeneration and repair in animal models [63] and humans [64-66]. Although other studies revealed the proliferative impact of PRP on Schwann cells [67,68], our results did not indicate a significant increase in the proliferation rate of Schwann cells after application of PRP alone or in combination with RVT at 48 and 72 hours.

Although our *in vitro* findings did not reveal significant improvements among experimental groups, *in vivo* results showed significant differences among experimental and negative control groups. In fact, the SFI and electrophysiological findings represented a significant improvement in both experimental groups in comparison with the negative control group. These results were comparable with vein graft [69] and autograft [70] in the similar animal model and follow-up periods. In accordance with other similar investigations [60, 70,71], application of nerve guide conduit significantly decreased latency time even compared to autograft group. This fact confirms the beneficial impact of nerve guide conduit utilization.

Compering our in vivo's results with previous studies shows that PU/GNF/Schwann cell/PRP/Resveratrol has suitable properties and it can be used to enhance sciatic nerve regeneration. Our results indicated SFI of -63.3±3.15 and -41.4±1.49 after 4 and 8 weeks respectively. Salehi et al. prepared conduit from polyurethane and gelatin nanofibrils and filled with melatonin and platelet-rich plasma and used for sciatic nerve defect of Wistar rat [72]. They reported SFI of -70.17±3.20 after 4 weeks and -56.90±2.01 after 8 weeks. It seems that resveratrol can enhance sciatic nerve injury better than melatonin. The hot plate latency of PU/GNF/Schwann cell/PRP/Resveratrol was 7 s. Whereas Mohammadi *et al*. investigated the neurodegenerative properties of poly(e-caprolactone)/collagen/nanobioglass nanofibrous conduits loaded with NGF, on sciatic nerve regeneration in Wistar rats reported hot plate latency of 7.5 s after 8 weeks [73]. It seems that resveratrol can help to improve sciatic nerve regeneration better than NGF.

In the current study, we found remarkable myelin sheath regeneration and more resemblance to the normal nerve in the application of conduit and RVT at the same time. These findings are in line with Bagriyanik *et al.* results which indicated a significant improvement in axon diameter and myelin thickness after application of RVT in the injured sciatic nerve of rats. In addition, the muscular damage was significantly diminished and recovered muscle mimic the normal gastrocnemius when conduit applied in combination

with RVT (group 2) compared with other experimental and negative control groups which revealed the positive impact of RVT for nerve recovery.

Conclusion

In the present study, we fabricated and evaluated a polyurethane/gelatin nanofibers conduit in combination with SCs, RVT, and PRP that can successfully promote injured sciatic nerve regeneration. Our *in vitro* and *in vivo* results represented PU/GNF/Schwann cell/PRP/Resveratrol conduits as a potential biocompatible nerve guide that enhanced recovery rate and functional abilities in the injured animal model.

References

1. J. S. Belkas, M. S. Shoichet, and R. Midha, *Neurol. Res.*, **26**, 151 (2004).
2. J. Noble, C. A. Munro, V. S. Prasad, and R. Midha, *J. Trauma Acute Care Surgery*, **45**, 116 (1998).
3. T. Hausner, R. Schmidhammer, S. Zandieh, R. Hopf, A. Schultz, S. Gogolewski, H. Hertz, and H. Redl in "How to Improve the Results of Peripheral Nerve Surgery", p.69, Springer, 2007.
4. R. V. Bellamkonda, *Biomaterials*, **27**, 3515 (2006).
5. G. R. Evans, *The Anatomical Record*, **263**, 396 (2001).
6. C. Chalfoun, G. Wirth, and G. Evans, *J. Cellular Mol. Med.*, **10**, 309 (2006).
7. N. Zhang, H. Yan, and X. Wen, *Brain Res. Rev.*, **49**, 48 (2005).
8. S. Farzamfar, M. Naseri-Nosar, A. Vaez, F. Esmaeilpour, A. Ehterami, H. Sahrapeyma, H. Samadian, A.-A. Hamidieh, S. Ghorbani, and A. Goodarzi, *Cellulose*, **25**, 1229 (2018).
9. M. Salehi, M. Naseri-Nosar, S. Ebrahimi-Barough, M. Nourani, A. Khojasteh, A. A. Hamidieh, A. Amani, S. Farzamfar, and J. Ai, *J. Biomed. Mater. Res. Part B: Appl. Biomat.*, **106**, 1463 (2018).
10. G. C. de Ruiter, M. J. Malessy, M. J. Yaszemski, A. J. Windebank, and R. J. Spinner, *Neurosurgical Focus*, **26**, E5 (2009).
11. J. Baier Leach, K. A. Bivens, C. W. Patrick Jr, and C. E. Schmidt, *Biotechnol. Bioeng.*, **82**, 578 (2003).
12. C. B. Herbert, C. Nagaswami, G. D. Bittner, J. A. Hubbell, and J. W. Weisel, *J. Biomed. Mater. Res. Part A*, **40**, 551 (1998).
13. J. C. Schense, J. Bloch, P. Aebischer, and J. A. Hubbell, *Nat. Biotechnol.*, **18**, 415 (2000).
14. N. Dubey, P. Letourneau, and R. Tranquillo, *Exp. Neurol.*, **158**, 338 (1999).
15. L. Binan, C. Tendey, G. De Crescenzo, R. El Ayoubi, A. Ajji, and M. Jolicoeur, *Biomaterials*, **35**, 664 (2014).
16. P. H. Robinson, B. Van Der Lei, H. J. Hoppen, J. W. Leenslag, A. J. Pennings, and P. Nieuwenhuis, *Microsurgery*, **12**, 412 (1991).
17. W. Den Dunnen, I. Stokroos, E. Blaauw, A. Holwerda, A. Pennings, P. Robinson, and J. Schakenraad, *J. Biomed. Mater. Res. Part A*, **31**, 105 (1996).
18. V. R. Hentz, J. M. Rosen, S.-J. Xiao, K. C. McGill, and G. Abraham, *J. Hand Surg.*, **16**, 251 (1991).
19. A. L. Dellon and S. E. Mackinnon, *Plastic and Reconstructive Surgery*, **82**, 849 (1988).
20. H. Molander, Y. Olsson, O. Engkvist, S. Bowald, and I. Eriksson, *Muscle & Nerve*, **5**, 54 (1982).
21. G. Evans, K. Brandt, M. Widmer, L. Lu, R. Meszlenyi, P. Gupta, A. Mikos, J. Hodges, J. Williams, and A. Gürlek, *Biomaterials*, **20**, 1109 (1999).
22. T. Cui, Y. Yan, R. Zhang, L. Liu, W. Xu, and X. Wang, *Tissue Eng. Part C: Methods*, **15**, 1 (2008).
23. L. Tian, M. P. Prabhakaran, and S. Ramakrishna, *Regenerative Biomaterials*, **2**, 31 (2015).
24. J. Chen, R. Dong, J. Ge, B. Guo, and P. X. Ma, *ACS Appl. Mater. Interfaces*, **7**, 28273 (2015).
25. L. Ghasemi-Mobarakeh, M. P. Prabhakaran, M. Morshed, M.-H. Nasr-Esfahani, and S. Ramakrishna, *Biomaterials*, **29**, 4532 (2008).
26. X. Liu, L. A. Smith, J. Hu, and P. X. Ma, *Biomaterials*, **30**, 2252 (2009).
27. R. Parenteau-Bareil, R. Gauvin, and F. Berthod, *Materials*, **3**, 1863 (2010).
28. S. Farzamfar, A. Ehterami, M. Salehi, A. Vaeez, A. Atashi, and H. Sahrapeyma, *J. Mol. Neurosci.,* 1 (2018).
29. W. Lu, M. Ma, H. Xu, B. Zhang, X. Cao, and Y. Guo, *Mater. Lett.*, **140**, 1 (2015).
30. H. Liu, X. Ding, G. Zhou, P. Li, X. Wei, and Y. Fan, *Journal of Nanomaterials*, **2013**, 3 (2013).
31. X. Wang, B. Ding, and B. Li, *Materials Today*, **16**, 229 (2013).
32. M. Salehi, M. Naseri Nosar, A. Amani, M. Azami, S. Tavakol, and H. Ghanbari, *Int. J. Polym. Mater. Polym. Biomater.*, **64**, 675 (2015).
33. L. A. Pfister, M. Papaloïzos, H. P. Merkle, and B. Gander, *J. Peripheral Nervous System*, **12**, 65 (2007).
34. A. Quincozes-Santos, A. C. Andreazza, P. Nardin, C. Funchal, C. A. Goncalves, and C. Gottfried, *Neurotoxicology*, **28**, 886 (2007).
35. P. Marambaud, H. Zhao, and P. Davies, *J. Biol. Chem.*, **280**, 37377 (2005).
36. G. Tredici, M. Miloso, G. Nicolini, S. Galbiati, G. Cavaletti, and A. Bertelli, *Drugs Exp. Clin. Res.*, **25**, 99 (1999).
37. H. D. Wang, Y. M. Shi, L. Li, J. D. Guo, Y. P. Zhang, and S. X. Hou, *British J. Pharmacol.*, **170**, 796 (2013).
38. H. Bagriyanik, N. Ersoy, C. Cetinkaya, E. Ikizoglu, D. Kutri, T. Ozcana, L. Kamanga, and M. Kiray, *Neurosci. Lett.*, **561**, 123 (2014).
39. T. Y. Farrag, M. Lehar, P. Verhaegen, K. A. Carson, and P. J. Byrne, *The Laryngoscope*, **117**, 157 (2007).
40. S. Abbasipour-Dalivand, R. Mohammadi, and V. Mohammadi,

Bulletin of Emergency & Trauma, **3**, 1 (2015).
41. F. Frattini, F. R. Pereira Lopes, F. M. Almeida, R. F. Rodrigues, L. C. Boldrini, M. A. Tomaz, A. F. Baptista, P. A. Melo, and A. M. B. Martinez, *Tissue Engineering Part A*, **18**, 2030 (2012).
42. G. Malleret, U. Haditsch, D. Genoux, M. W. Jones, T. V. Bliss, A. M. Vanhoose, C. Weitlauf, E. R. Kandel, D. G. Winder, and I. M. Mansuy, *Cell*, **104**, 675 (2001).
43. A. Al-Hayani, *J. Taibah University Medical Sciences*, **2**, 4 (2007).
44. N. Sultana, M. I. Hassan, and M. M. Lim in "Composite Synthetic Scaffolds for Tissue Engineering and Regenerative Medicine", p.13, Springer, 2015.
45. F. Bastami, Z. Paknejad, M. Jafari, M. Salehi, M. R. Rad, and A. Khojasteh, *Mater. Sci. Eng.: C*, **72**, 481 (2017).
46. M. Naseri-Nosar, S. Farzamfar, H. Sahrapeyma, S. Ghorbani, F. Bastami, A. Vaez, and M. Salehi, *Mater. Sci. Eng.: C*, **81**, 366 (2017).
47. M. Salehi, S. Farzamfar, F. Bastami, and R. Tajerian, *Biomed. Eng.: Appl., Basis and Commun.*, **28**, 1650035 (2016).
48. J. P. Brockes, K. L. Fields, and M. C. Raff, *Brain Research*, **165**, 105 (1979).
49. L.-M. Chen, D. Bailey, and C. Fernandez-Valle, *The Journal of Neuroscience*, **20**, 3776 (2000).
50. M. Salehi, M. Naseri-Nosar, M. Azami, S. J. Nodooshan, and J. Arish, *Tissue Eng. Regener. Med.*, **13**, 498 (2016).
51. Y. Kajikawa, T. Morihara, H. Sakamoto, K. I. Matsuda, Y. Oshima, A. Yoshida, M. Nagae, Y. Arai, M. Kawata, and T. Kubo, *J. Cellular Physiol.*, **215**, 837 (2008).
52. J. R. Dijkstra, M. F. Meek, P. H. Robinson, and A. Gramsbergen, *J. Neurosci. Meth.*, **96**, 89 (2000).
53. J. P. Conry, L. B. Messer, J. C. Boraas, D. P. Aeppli, and T. Bouchard, *Archives of Oral Biology*, **38**, 937 (1993).
54. T. Olszowski, G. Adler, J. Janiszewska-Olszowska, K. Safranow, and M. Kaczmarczyk, *Oral Dis*, **18**, 389 (2012).
55. W. Zhang, A. MacFadyen, and P. Wang, *Astrophys. J. Lett.*, **692**, L40 (2009).
56. R. Muir, S. Weaver, J. Bradshaw, G. Eby, and J. Evans, *J. Geological Society*, **152**, 689 (1995).
57. Y.-T. Kao, C. Saxena, L. Wang, A. Sancar, and D. Zhong, *Proceedings of the National Academy of Sciences of the United States of America*, **102**, 16128 (2005).
58. V. Chiono, C. Tonda-Turo, and G. Ciardelli, *Int. Rev. Neurobiol.*, **87**, 173 (2009).
59. G. Ciardelli and V. Chiono, *Macromol. Biosci.*, **6**, 13 (2006).
60. M. Salehi, M. Naseri-Nosar, S. Ebrahimi-Barough, M. Nourani, A. Khojasteh, S. Farzamfar, K. Mansouri, and J. Ai, *Cellular and Molecular Neurobiology*, 1 (2017).
61. D. Funk, C. Fricke, and B. Schlosshauer, *Eur. J. Cell Biol.*, **86**, 207 (2007).
62. H. M. Chang, C. H. Liu, W. M. Hsu, L. Y. Chen, H. P. Wang, T. H. Wu, K. Y. Chen, W. H. Ho, and W. C. Liao, *J. Pineal Res.*, **56**, 322 (2014).
63. F. Bastami, P. Vares, and A. Khojasteh, *J. Craniofacial Surgery*, **28**, e49 (2017).
64. M.-A. Malahias, D. Chytas, G. C. Babis, and V. S. Nikolaou, *Frontiers in Surgery*, **1** (2014).
65. W. Yu, J. Wang, and J. Yin, *Int. J. Neurosci.*, **121**, 176 (2011).
66. A. Khojasteh, S. Hosseinpour, P. Nazeman, and M. Dehghan, *International Journal of Oral and Maxillofacial Surgery*, **45**, 1303 (2016).
67. J. B. Davis and P. Stroobant, *J. Cell Biol.*, **110**, 1353 (1990).
68. M. Sondell, G. Lundborg, and M. Kanje, *Journal of Neuroscience*, **19**, 5731 (1999).
69. R. Mohammadi, S. Azizi, N. Delirezh, R. Hobbenaghi, and K. Amini, *Chinese Journal of Traumatology (English Edition)*, **14**, 46 (2011).
70. M. Salehi, M. Naseri-Nosar, S. Ebrahimi-Barough, M. Nourani, A. Khojasteh, A. A. Hamidieh, A. Amani, S. Farzamfar, and J. Ai, *J. Biomed. Mater. Res. Part B: Appl. Biomat.*, **106**, 1463 (2018).
71. M. V. M. Ganga, J. Coutinho-Netto, B. O. Colli, W. Marques Junior, C. H. R. Catalão, R. T. Santana, M. R. P. Oltramari, K. T. Carraro, J.-J. Lachat, and L. D. S. Lopes, *Acta Cirurgica Brasileira*, **27**, 885 (2012).
72. M. Salehi, M. Naseri-Nosar, S. Ebrahimi-Barough, M. Nourani, A. Khojasteh, S. Farzamfar, K. Mansouri, and J. Ai, *Cell. Mol. Neurobiol.*, **38**, 703 (2018).
73. F. Mohamadi, S. Ebrahimi-Barough, M. R. Nourani, A. Ahmadi, and J. Ai, *Artificial Cells, Nanomedicine, and Biotechnology*, 1 (2018).